First-principles prediction of half-metallic ferromagnetic semiconductors: V- and Cr-doped BeTe

S. Picozzi
Istituto Nazionale di Fisica della Materia (INFM), Dipartimento di Fisica, Università degli Studi di L'Aquila, 67010 Coppito (L'Aquila), Italy

T. Shishidou and A. J. Freeman
Department of Physics and Astronomy and Materials Research Center, Northwestern University, Evanston, Illinois 60208

B. Delley
Paul Scherrer Institut WHGA/123, CH-5232 Villigen PSI, Switzerland

(Received 8 November 2002; revised manuscript received 21 January 2003; published 16 April 2003)

From results of first-principles all-electron full-potential linearized augmented plane-wave calculations, a materials design of half-metallic ferromagnetic semiconductors based on V- and Cr-doped BeTe is proposed. Without the need of *n*- or *p*-type doping, the stability of the ferromagnetic spin configuration versus the antiferromagnetic state for V- and Cr-based systems is predicted, whereas the situation is reversed for Mn-doped BeTe ordered alloys. The calculated electronic and magnetic structures of transition-metal-doped BeTe shows that consistent with the integer value for the total magnetic moment, half metallicity is obtained for V- and Cr- doped structures, whereas the Mn-doped systems are semiconducting. A careful analysis of the spin density reveals the antiferromagnetic (ferromagnetic) coupling between the Cr and V (Mn) *d* states and the anion dangling-bond *p* states, which is believed to be responsible for the stabilization of the ferromagnetic (antiferromagnetic) phase. These ferromagnetic semiconductors offer a potential for semiconductor spintronic applications at room temperature; therefore, an experimental confirmation of our theoretical predictions is encouraged.

DOI: 10.1103/PhysRevB.67.165203 PACS number(s): 75.50.Pp, 71.55.Gs, 71.20.Nr

I. INTRODUCTION

The attractive idea of manipulating the spin of the electron, in addition to its charge, as an added degree of freedom continues to stimulate intense interest in the field "spintronics."[1–5] Within this framework, the discovery of ferromagnetic materials operating at room temperature and with high-thermal equilibrium stability would be a breakthrough in realizing spin-polarized transistors, or in integrating spin-logic and nonvolatile spin memory into the exciting field of quantum computing. So far, most of the work has focused on (Ga,Mn)As or (In,Mn)As diluted magnetic semiconductors (DMS),[2] with transition temperatures up to 110 K. However, the solubility of 3*d* transition metals (TMs) in standard III-V semiconductors is extremely low ($<7\%-8\%$), so that high operating Curie temperatures seem to be difficult to reach with current synthesis techniques. On the other hand, the large solubility of 3*d* TMs in II-VI semiconductors (of the order of 10%–25% (Ref. 6) and the opportunity to independently control the localized spin (supplied by the magnetic impurities) and the hole concentration (typically achieved by nitrogen doping) also makes them particularly attractive for fundamental studies.[7,8] In particular, in the search for new DMS having high Curie temperatures and whose magnetic properties are controllable by changing the carrier density, a materials design based on first-principles calculations was performed for TM-doped Zn-based II-VI compounds.[9,10] It was proposed that ferromagnetic DMS with high Curie temperatures can be realized using ZnS, ZnSe, and ZnTe doped with V or Cr and ZnO-based DMS doped with Fe, Co, Ni, V, and Cr.

It was recently reported[11] that high quality films of *p*-type BeMnTe, almost lattice matched to GaAs, could be grown by solid source molecular-beam epitaxy for Mn concentrations up to 10%. For highly nitrogen-doped samples (3.4×10^{19} cm^{-3}), a hysteretic behavior of the anomalous Hall effect was observed, indicating a ferromagnetic state below 3 K; it was further suggested that a sizeable increase in doping with an optimized plasma source should lead to an increase in the Curie temperature, T_C. Since there are fundamental difficulties[12] in injecting spin-polarized electrons into a common semiconductor from a ferromagnetic metal, it seems easier to find a ferromagnetic semiconductor with a smaller conductivity than metals and 100% spin polarization, which can be grown on common semiconductors. Within this framework, we point out that the already small lattice mismatch (0.46%) between BeTe (with lattice constant $a^{\mathrm{BeTe}}=10.63$ a.u.) and GaAs ($a^{\mathrm{GaAs}}=10.68$ a.u.) could even be reduced by the introduction of a small amount of Mn, thereby improving the quality of the (Be,*TM*)Te epilayers.

Stimulated by this recent experimental work, we performed accurate first-principles calculations within density-functional theory in the generalized gradient approximation (GGA) for zinc-blende BeTe doped with different 3*d* magnetic impurities, such as V, Cr, and Mn. In Sec. II and Sec. III, we report the computational and structural details; in Sec. IV we discuss the electronic and magnetic properties in terms of the density of states, favored spin configurations, and magnetic moments; and in Sec. V we draw conclusions.

II. COMPUTATIONAL DETAILS

The theoretical framework on which our predictions are based is spin-polarized density-functional theory. Since it

was shown that the local-spin-density approximation (LSDA) to the exchange-correlation potential[13] in DMS can severely underestimate equilibrium lattice constants and bond lengths between the $3d$ element and the anions,[14] we used the GGA, following the Perdew-Burke-Ernzerhof scheme.[15] Two different *ab initio* codes, namely, density-functional theory for molecules and three-dimensional periodic solids[16] (DMol^3) and full-potential linearized augmented plane-wave (FLAPW)[17] methods are used.

An efficient three-dimensional numerical integration of the matrix elements occurring in the Ritz variational method and the choice of localized numerical orbitals, used as a basis set, are at the basis of the high level of accuracy of the DMol^3 results. Scalar relativistic effects are included via a local pseudopotential for all-electron calculations.[18] Here, a double set of numerical valence functions with a local basis cutoff R_c of 11.0 a.u. is used. The structural degrees of freedom (internal relaxations) are optimized using DMol^3 and the final equilibrium geometry is refined using the highly accurate FLAPW method.

The FLAPW approach is considered to be the most accurate *ab initio* electronic structure method, in which there is no artificial shape approximation for the wave functions, charge density, and potential. In this work, we have used the FLAPW parallel implementation.[19] For all atoms, the core and valence states are treated fully- and semirelativistically (i.e., without spin-orbit coupling), respectively. The muffin-tin radii for V, Cr, and Mn are set equal to 2.3 a.u., and 2.5 and 2.0 a.u. are used for Te and Be, respectively. A cutoff of 3.4 a.u. was employed for the wave-function expansion in the interstitial region, whereas a 9-a.u. cutoff was used for the charge density and potential. Integrations in reciprocal space are performed following the Monkhorst-Pack scheme,[20] using a set of six special **k** points in the irreducible wedge of the Brillouin zone. Tests performed on the $TM_{0.25}Be_{0.75}Te$ case have shown that, by increasing the number of **k** points to 18, there were no remarkable differences in the relevant properties (such as magnetic moments and density of states): the property most sensitive to the computational details, i.e., the difference between the total energies in the ferromagnetic and antiferromagnetic spin configurations, varied by about 15 meV/TM atom, and is thus considered as our numerical precision (see below). The density of states were obtained according to the tetrahedron scheme[21] for the Brillouin-zone sampling, using a set of 40 **k** points in the irreducible part of the zone.

III. STRUCTURAL DETAILS

We consider different concentrations (namely, 25%, 12.5%, and 6.25% with 16, 32, and 64 atoms per unit cell, respectively) of TMs substituting for the Be cation in $TM_xBe_{1-x}Te$ (TM=V, Cr, Mn) systems. In order to mimic the experimental growth along the [001] axis, we constrain the experimental in-plane lattice constant to that of GaAs,[22] $a=10.68$ a.u., which is different by less than 0.4% from the BeTe experimental lattice constant ($a=10.63$ a.u.),[23] so that the small strain within the BeTe host matrix can be neglected. Note that our BeTe calculated lattice constant is 10.71 and 10.52 a.u. within the GGA and local-density approximation, respectively, and thus yields good agreement ($+0.75\%$ and -1.03%) with experiment for both exchange-correlation functionals. The out-of-plane lattice parameter (i.e., parallel to the [001] axis) is taken as the FLAPW-calculated average over composition of those in tetragonal BeTe and TMTe, strained on a GaAs substrate: for example, in the 25% case, the tetragonal c/a ratio (equal to 1 in the ideal cubic case, such as BeTe strained on GaAs) in the superlattice (SL) is set as $c/a^{\mathrm{SL}}=[3(c/a)^{\mathrm{BeTe}}+(c/a)^{\mathrm{TMTe}}]/4$. The calculated c/a ratios for [001] ordered tetragonal VTe, CrTe, and MnTe (i.e., $x=1.0$) are 1.28, 1.29, and 1.28 for ferromagnetic (FM) and 1.27, 1.27, and 1.25 for antiferromagnetic (AFM) alignments. Since the c/a value in the three TM tellurides depends very slightly on the TM and on the spin configurations, we take an average value $c/a^{\mathrm{TMTe}}=1.275$. (Incidentally, we note that ferromagnetism is the stable spin configuration for V and Cr tellurides and it is antiferromagnetism for MnTe.)

TABLE I. DMol^3 calculated total-energy difference, Δ_{FA} (in meV/TM), between the ferromagnetic and antiferromagnetic spin states as a function of the TM concentration, x.

x	0.25	0.125		0.0625
		I	II	
$V_xBe_{1-x}Te$	-106	-122	-12	~ 0
$Cr_xBe_{1-x}Te$	-39	-29	$+7$	-10
$Mn_xBe_{1-x}Te$	$+34$	$+31$	$+3$	~ 0

Moreover, we checked the accuracy of the GGA functional, by calculating the MnTe equilibrium lattice constant in the zinc-blende phase.[24] The calculated values are $a_{\mathrm{LSDA}}^{\mathrm{MnTe}}=11.45$ a.u. and $a_{\mathrm{GGA}}^{\mathrm{MnTe}}=11.88$ a.u. within LSDA and GGA, respectively, to be compared with the experimental value, $a_{exp}^{\mathrm{MnTe}}=11.96$ a.u.[25] We point out that (i) GGA better reproduces the experimental lattice constant, (ii) GGA corrects the well-known LSDA ''overbinding,'' by giving lattice constants larger by a few percent, and (iii) our results are in excellent agreement with previous LSDA first-principles calculations that give the MnTe equilibrium lattice constant $a=11.5$ a.u.[26]

For the $x=0.125$ case, we considered two different Mn configurations: in the first [denoted as 0.125(I)], the two Mn atoms are located at the origin and at the center of the tetragonal cell; in the second [denoted as 0.125(II)], the first Mn atom is located at the cell origin and the second Mn sits above the first one (i.e., same x and y coordinates), having its z coordinate equal to half of the unit-cell Bravais vector along the c axis. The internal degrees of freedom in the SL are fully relaxed according to *ab initio* atomic forces, yielding the equilibrium geometry.

IV. RESULTS AND DISCUSSION

A. Magnetic alignments

We focus first on the stability of the spin configurations, and show in Table I the FLAPW calculated total-energy dif-

ference (Δ_{FA}) between the FM and AFM configuration (i.e., negative numbers denote FM stability). Incidentally, we note that the DMol^3 results are consistent (within our numerical uncertainty, estimated as 15 meV/TM atom on Δ_{FA}) with the FLAPW results, giving evidence of the good accuracy of the DMol^3 calculations.

What is remarkable in Table I is that the Mn-doped systems show antiferromagnetism as the favored spin configuration, whereas Cr– and V–doped systems show ferromagnetism. Let us now focus on the exchange mechanisms proposed for DMS and discuss how our results can be explained according to these interactions. Recall that the double-exchange model,[27] proposed by Zener,[28] couples magnetic ions in different charge states by virtual hopping of the ''extra'' electron from one ion to the other. Within the band-structure framework, this means that near half filling and when the exchange splitting is larger than the bandwidth, the band energy of the FM state is lower than that of the AFM spin configuration if a sufficient number of holes (usually small) is present. This mechanism is believed to stabilize the ferromagnetism in the manganites with perovskite structure, such as $LaMnO_3$, upon hole doping. On the other hand, the superexchange mechanism,[29,30] resulting from the *sp-d* hybridization, is a process in which the spins of two ions are correlated due to the spin-dependent kinetic exchange interaction between each of the two ions and the valence *p* band. Within the band-structure framework, superexchange originates from the downward shift of the split *d* bands, which lowers the band energy in the AFM state. Our results for V– and Cr-doped systems are fully consistent with the general idea of ferromagnetism driven by a double-exchange interaction that overcomes the antiferromagnetic superexchange interaction. On the other hand, in the case of Mn, antiferromagnetic superexchange becomes dominant with no contribution from the ferromagnetic double exchange for an insulator or semiconductor (this will be discussed in greater detail in the following, which focuses on the density of states).

Let us now compare our results with available experimental data. As already pointed out, it was shown experimentally that Mn–doped II-VI semiconductors can show ferromagnetism upon hole doping.[7,8] In particular, the AFM coupling between Mn spins in undoped BeTe samples was reported to be overcome by the hole–mediated FM interaction when the N-dopant concentration is increased up to 3.4×10^{-19} cm^{-3}. These findings are consistent with our results: the AFM coupling is in fact confirmed in undoped MnBeTe. Moreover, our calculations clearly show that Cr- and V-based systems show ferromagnetism without *n*- or *p*-type doping.

In all three TM-based systems, Δ_{FA} decreases as the TM concentration increases; this is in agreement with that previously obtained from first-principles Korringa-Kohn-Rostoker calculations with the coherent-potential approximation for other II-VI Zn-based semiconductors.[31] This trend seems to suggest that the magnetic interactions are quite short ranged.

Let us compare our results with those obtained for the more studied GaMnAs, in terms of the FLAPW calculated Δ_{FA} (Ref. 32) at the same TM concentration as those reported here. In the case of GaMnAs, Δ_{FA} is of the order of 120–170 meV/atom, thus suggesting Mn-doped III-V compounds as slightly more promising. However, it is well known that Mn clustering occurs for TM concentrations higher than 10% in GaAs and that the presence of antisites or interstitial Mn lowers the stability of the FM spin configuration. On the other hand, the higher solubility of the TM atoms in a II-VI matrix should make feasible the incorporation of higher concentrations of Cr and V dopants within BeTe, resulting in the strong stability of the FM spin configuration. $Cr_xBe_{1-x}Te$ and $V_xBe_{1-x}Te$ alloys can therefore be considered as potentially good candidates for room-temperature ferromagnetism.

B. Density of states

In Fig. 1, we show the FLAPW-calculated total density of states (DOS) and the TM projected density of states (PDOS) for BeVTe, BeCrTe, and BeMnTe in the $x=0.25$ case for the FM and AFM spin configurations. The total DOS in the FM case shows that the Mn-based system is a semiconductor (i.e., no states are available at E_F), whereas the Cr- and V-based alloys are half metallic [i.e., spin-up (-down) states are available (not available) at the Fermi level, E_F]. In the AFM spin configuration, the semiconducting character is kept by the Mn-doped system, whereas both Cr- and V-doped structures show metallic character.

As far as the TM PDOS is concerned, we observe that the spin-down states for all three TM are mostly unoccupied, following a trend common to most DMS;[33] on the other hand, there are marked differences between Mn, Cr, and V in the spin–up states DOS. In particular, according to Zunger,[34] the electronic structure of a TM which substitutes a cation in a zinc-blende semiconductor can be described by a hybridization mechanism between the TM orbitals and the anion dangling bonds—mainly with *p* character—formed by a cation vacancy in the host matrix.[35] As a result, the e_g (Ref. 36) states essentially retain their well-localized atomiclike character and, are therefore, nonbonding; the t_{2g} states, on the other hand, form delocalized bonding $(t_{2g})_b$ and antibonding $(t_{2g})_a$ states. The approximate energy position of these states are marked in Fig. 1 for all three TM projected densities of states.

The decreased splitting in energy between the $(t_{2g})_b$ and e_g states and the increased splitting between the e_g and $(t_{2g})_a$ states in going from V to Cr to Mn is consistent with an expected trend: as the atomic number increases, the $3d$ orbital energy decreases and the hybridization with the vacancy state is increasingly weakened. In particular, in the Mn case, the $(t_{2g})_a$ state lies below E_F, whereas in the Cr- and V-based structures, the $(t_{2g})_a$ state is pushed into the band gap of the nondoped BeTe, so as to lie just in proximity to E_F in the TM-doped systems. As mentioned above, according to the so-called generalized ferromagnetic double-exchange interaction,[27] the partially occupied $(t_{2g})_a$ band can lower the total energy, so as to stabilize the FM spin configurations; our results, see Figs. 1(b) and 1(c), are therefore consistent with this interpretation. Moreover, we expect that an even stronger stabilization of the FM ordering would

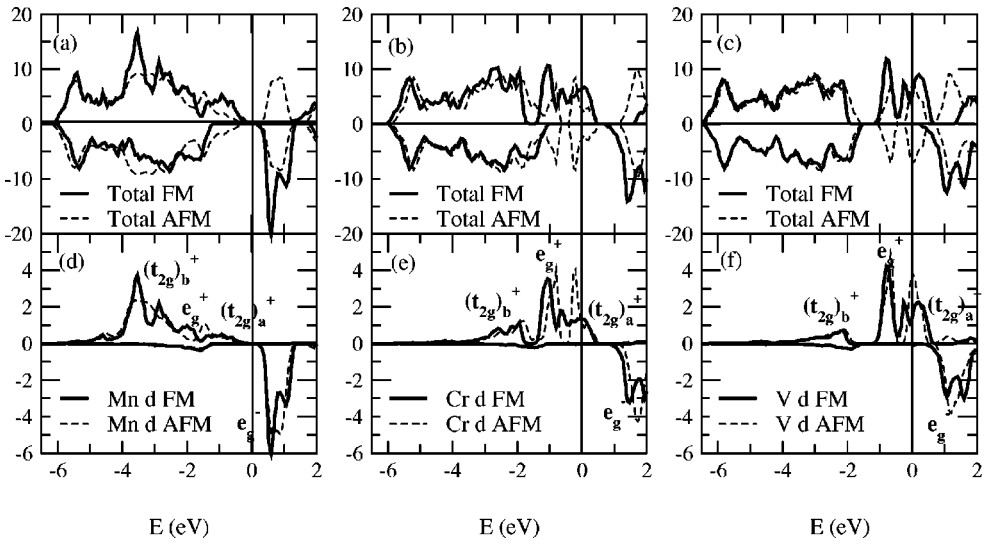

FIG. 1. FLAPW calculated density of states for the FM (solid) and AFM (dashed) spin configurations at $x = 0.25$: (a) BeMnTe total DOS, (b) BeCrTe total DOS, (c) BeVTe total DOS, (d) BeMnTe Mn *d* PDOS, (e) BeCrTe Cr *d* PDOS, and (f) BeVTe V *d* PDOS. The Fermi level is set to zero in the energy scale. A Gaussian smearing of 0.1 eV is used.

occur upon hole doping, therefore increasing the Curie temperature and suggesting these materials as good candidates for spintronic room-temperature applications.

The exchange splitting, estimated as the difference between the nonhybridized e_g^+ and e_g^- states, is about 3.2 eV, 2.5 eV, and 2.0 eV for Mn, Cr, and V, respectively, and follows the expected trend as a function of the number of *d* electrons. In all cases, the crystal-field splitting (defined as the energy difference between the e_g and t_{2g} states) is smaller than the exchange splitting, so that the high-spin ground state is stabilized. Finally, we point out that similar features were theoretically observed in the case of other TM-doped II-VI compounds, such as ZnS, ZnSe, and ZnTe.[31]

As far as the comparison between the TM PDOS in the FM and AFM spin configurations, note that for the Mn PDOS, the FM bandwidth is slightly larger than that in the AFM configuration. We can explain this trend as follows: in the FM state, the Mn *d* band is widened by hybridization between spin-up states, whereas this mechanism is prohibited in the AFM configuration, where neighboring Mn sites have opposite spins. Moreover, if we estimate the center of gravity of the spin-up *d* band, we find, according to an efficient superexchange interaction, that its energy is lower in the AFM configuration compared to the FM case, so that the band energy is lowered and the AFM spin state is stabilized.

C. Magnetic properties

We show in Table II the FLAPW-calculated magnetic moments for a fixed TM concentration ($x = 0.25$) for the FM and AFM spin configurations. The total integer magnetic moments are consistent with both the half-metallic character shown by the total DOS (see Fig. 1) and the number of holes and the total magnetic moments obtained by integration of the spin-resolved total density of states (not shown). In Mn-doped DMS, it is expected[33] that (i) the number of valence minority-spin electrons is not changed by the Mn impurity and (ii) each Mn impurity adds five additional majority-spin states to the valence band. Table II shows that this picture is valid also in Mn-doped BeTe: since Mn (Be) has seven (two) valence electrons, there will be five net electrons contributed by each Mn substituting for Be to fill the majority-spin band. As a result, we expect (and indeed find) that every Mn impurity adds no hole carriers ($N_h = 0$) to the otherwise perfect BeTe crystal and that the total magnetic moment amounts to $5\mu_B$. Within this same framework, each Cr (V) provides six (five) valence electrons, so that there will only be four (three) net electrons contributed by the TM substituting for Be to fill the up-spin band; it follows that every Cr (V) adds one (two) hole carriers and the total magnetic moment per TM impurity equals $4\mu_B$ $(3\mu_B)$.

The TM magnetic moment decreases in going from Mn to Cr to V, consistent with the trend for the total magnetic moment; the strong similarity shown by the FM and AFM spin configurations suggests that the TM magnetic moments are weakly coupled, even with the relatively high concentration ($x = 0.25$) of magnetic impurities. What we need to stress is the different sign of the induced magnetic moment on the nearest–neighbor (nn) anion: in the case of Mn, the TM-nn Te moment is positive, whereas for Cr and V it is negative. It was suggested that a negative spin polarization could be a signature of the AFM coupling between the polarized hole

TABLE II. FLAPW calculated magnetic moments for $x = 0.25$: total/(TM atom), TM, TM-nn Te, and TM-second-nearest-neighbor Be. All values are in Bohr magnetons.

	$Mn_{0.25}Be_{0.75}Te$		$Cr_{0.25}Be_{0.75}Te$		$V_{0.25}Be_{0.75}Te$	
	FM	AFM	FM	AFM	FM	AFM
μ^{tot}	5	0	4	0	3	0
μ^{TM}	3.82	± 3.79	3.19	± 3.16	2.40	± 2.39
μ^{Te}	0.05	± 0.03	-0.04	∓ 0.04	-0.03	∓ 0.03
μ^{Be}	0.03	0	0.03	0	0.03	0

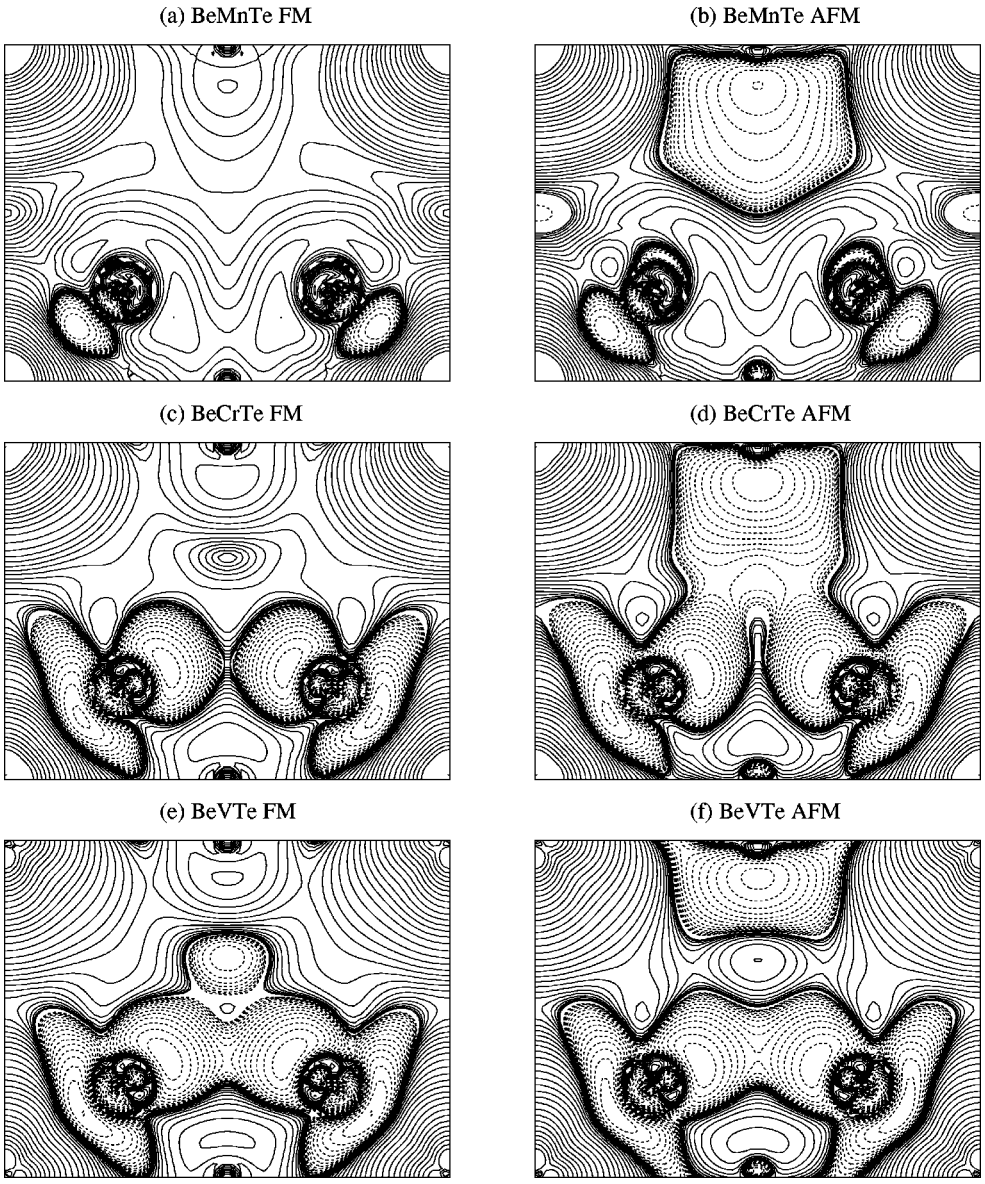

FIG. 2. FLAPW calculated spin-density contour plots in the [110] plane for (a) FM BeMnTe, (b) AFM BeMnTe, (c) FM BeCrTe, (d) AFM BeCrTe, (e) FM BeVTe, and (f) AFM BeVTe. Contour plots start at 1×10^{-4} e/a.u.^{3} and increase successively by a factor of $2^{1/2}$. Positive (negative) spin density is represented by solid (dashed) lines. The TM is located at the corners of each panel and is bonded to Te; the next-nearest-neighbor Be is located half way along the horizontal edges.

and the Mn spin in the model[5] proposed by Dietl *et al.* to explain diluted magnetic semiconductor ferromagnetism. It was also argued[32] that in Mn-doped magnetic semiconductors, the antiferromagnetic interaction between Mn $3d$ and its nearest-neighbor anion p states could lower the total energy, thereby stabilizing the ferromagnetic alignment.

Our present results are consistent with these models: the ferromagnetic (antiferromagnetic) alignment is strongly favored when the induced anion spin polarization is negative (positive). In order to clarify this issue, we show in Fig. 2 the spin-density contour plots for the TM-Te-Be bonds in the FM and AFM spin configurations for the three different TM–doped systems with $x = 0.25$. The plane shown in Fig. 2 contains only up-spin TM atoms (located at the corners of the panels), both in the FM and AFM configurations. Except for the BeMnTe system, there is mostly p-like negative spin density at the Te atoms, whereas the Be atoms (located half way along the horizontal edges) are positively spin polarized in the FM case and show a positive (negative) spin polarization in the positive (negative) growth direction (i.e., vertical edges of the panels). The spin density is remarkably different in proximity to the Te atoms and TM-Te bonds for systems in which the FM alignment is favored compared to systems favoring the AFM alignment: a negative cloud is present in the case of Cr and V, whereas Mn only shows a very small negative polarization along the Mn-Te bonds, the anion being positively spin polarized overall. Moreover, in comparing the FM spin-density contour plots for the different metals, we notice a trend as a function of the TM: the negative spin-density region around the anion increases in going from Mn to Cr to V, consistent with the increase in Δ_{FA}.

V. CONCLUSIONS

Using an accurate first–principles approach, we have predicted half-metallic ferromagnetism in V- and Cr-doped BeTe, without the need for n- or p-type doping; this offers the opportunity to investigate the potential of BeCrTe and BeVTe ferromagnetic alloys as basic materials in spintronic devices. On the other hand, Mn-doped systems show AFM as

the favored spin configuration and semiconducting behavior. We have given a detailed analysis of the electronic and magnetic properties of these ordered alloys, in terms of density of states, magnetic moments, and total-energy differences. Our results show that the difference in total energy between the spin configurations considered, Δ_{FA}, decreases with the TM concentration, consistent with quite short-ranged magnetic interactions. The electronic and magnetic properties result from the interplay between the exchange splitting, the crystal-field splitting, and the hybridization of TM *d* states with dangling-bond anion *p* states. The differences in the total DOS and in the TM PDOS can be interpreted within a generalized double-exchange interaction that stabilizes the FM phase in V- and Cr-doped BeTe alloys, whereas the only active mechanism in the Mn-based system is superexchange, therefore stabilizing, in the absence of any other additional dopants, the AFM configuration.

ACKNOWLEDGMENT

Work at Northwestern University is supported by DARPA–ONR Grant No. N00014-02-1-0887.

[1] Y. D. Park, A. T. Hanbicki, S. C. Erwin, C. S. Hellberg, J. M. Sullivan, J. E. Mattson, T. F. Ambrose, A. Wilson, G. Spanos, and B. T. Jonker, Science **295**, 651 (2002), and references therein.

[2] H. Ohno, Science **281**, 951 (1998).

[3] Y. Ohno, D. K. Young, B. Beschoten, F. Matsukura, H. Ohno, and D. D. Awschalom, Nature (London) **402**, 790 (1999).

[4] R. Fiederling, M. Keim, G. Reuscher, W. Ossau, G. Schmidt, A. Waag, and L. W. Molenkamp, Nature (London) **402**, 787 (1999).

[5] T. Dietl, H. Ohno, F. Matsukura, J. Cibert, and D. Ferrand, Science **287**, 1019 (2000).

[6] J. K. Furdyna, J. Appl. Phys. **64**, R29 (1988).

[7] A. Haury, A. Wasiela, A. Arnoult, J. Cibert, S. Tatarenko, T. Dietl, and Y. Merle d'Aubigné, Phys. Rev. Lett. **79**, 511 (1997).

[8] D. Ferrand, J. Cibert, C. Bourgognon, S. Tatarenko, A. Wasiela, G. Fishman, A. Bonanni, H. Sitter, S. Kolesnik, J. Jaroszynski, A. Barcz, and T. Dietl, J. Cryst. Growth **214/215**, 387 (2000).

[9] K. Sato and H. Katayama-Yoshida, Phys. Status Solidi B **229**, 673 (2002).

[10] K. Sato and H. Katayama-Yoshida, Semicond. Sci. Technol. **17**, 367 (2002).

[11] L. Hansen, D. Ferrand, G. Richter, M. Thierley, V. Hock, N. Schwarz, G. Reuscher, G. Schmidt, L. W. Molenkamp, and A. Waag, Appl. Phys. Lett. **79**, 3125 (2001).

[12] G. Schmidt, D. Ferrand, L. W. Molenkamp, A. T. Filip, and B. J. van Wees, Phys. Rev. B **62**, R4790 (2000).

[13] U. Von Barth and L. Hedin, J. Phys. C **5**, 1629 (1972).

[14] A. Continenza, S. Picozzi, W. T. Geng, and A. J. Freeman, Phys. Rev. B **64**, 085204 (2001).

[15] J. P. Perdew, K. Burke, and M. Ernzerhof, Phys. Rev. Lett. **77**, 3865 (1996).

[16] B. Delley, J. Chem. Phys. **113**, 7756 (2000); **92(1)**, 508 (1990).

[17] E. Wimmer, H. Krakauer, M. Weinert, and A. J. Freeman, Phys. Rev. B **24**, 864 (1981); H. J. F. Jansen and A. J. Freeman, *ibid.* **30**, 561 (1984).

[18] B. Delley, Int. J. Quantum Chem. **69**, 423 (1998).

[19] A. Canning, W. Mannstadt, and A. J. Freeman, Comput. Phys. Commun. **130**(3), 233 (2000); T. Shishidou and A. J. Freeman (unpublished).

[20] H. J. Monkhorst and J. D. Pack, Phys. Rev. B **13**, 5188 (1976).

[21] G. Gilat and L. J. Raubenheimer, Phys. Rev. **144**, 390 (1966); O. Jepsen and O. K. Andersen, Solid State Commun. **9**, 1763 (1971); G. Lehmann and M. Taut, Phys. Status Solidi B **54**, 469 (1972).

[22] B. G. Streetman, *Solid State Electronic Devices*, 3rd ed. (Prentice-Hall, Englewood Cliffs, NJ, 1990).

[23] A. Munoz, P. Rodriguez-Hernandez, and A. Mujica, Phys. Rev. B **54**, 11 861 (1996), and references therein.

[24] We chose MnTe as a test compound since, to our knowledge, no experimental lattice constants are available for CrTe and VTe in the zinc-blende structure.

[25] J. K. Furdyna, J. Appl. Phys. **64**, R29 (1988).

[26] I. Galanakis and P. Mavropoulos, Phys. Rev. B **67**, 104417 (2003).

[27] H. Akai, Phys. Rev. Lett. **81**, 3002 (1998).

[28] C. Zener, Phys. Rev. **82**, 403 (1951).

[29] B. E. Larson, K. C. Hass, H. Ehrenreich, and A. E. Carlsson, Phys. Rev. B **37**, 4137 (1988).

[30] *Diluted Magnetic Semiconductors*, edited by J. K. Furdyna and J. Kossut, Semiconductor and Semimetals Vol. 25 (Academic, New York, 1988).

[31] K. Sato and H. Katayama-Yoshida, Jpn. J. Appl. Phys., Part 2 **40**, L651 (2001).

[32] Y. J. Zhao, W. T. Geng, K. T. Park, and A. J. Freeman, Phys. Rev. B **64**, 035207 (2001).

[33] T. C. Schulthess and W. H. Butler, J. Appl. Phys. **89**, 7021 (2001).

[34] A. Zunger, in *Solid State Physics*, edited by F. Seitz and D. Turnbull (Academic, New York, 1986), Vol. 39, p. 275.

[35] F. Beeler, O. K. Andersen, and M. Scheffler, Phys. Rev. B **41**, 1603 (1990).

[36] Although for an arbitrary **k** point, the wave function does not belong to a single irreducible representation, it is useful to keep this notation for the bands originally formed by e_g and t_{2g} orbitals.